Redox Biology 64 (2023) 102792

Contents lists available at ScienceDirect

Redox Biology

journal homepage: www.elsevier.com/locate/redox

Click chemistry-based thiol redox proteomics reveals significant cysteine reduction induced by chronic ethanol consumption

Peter S. Harris, Courtney D. McGinnis, Cole R. Michel, John O. Marentette, Richard Reisdorph, James R. Roede, Kristofer S. Fritz *

Skaggs School of Pharmacy and Pharmaceutical Sciences, University of Colorado Anschutz Medical Campus, Aurora, CO, 80045, USA

ARTICLE INFO

Keywords:
Cysteine
Thiol
Redox
Proteomics
Alcohol-associated liver disease
Mass spectrometry
Click chemistry
Glutathione

ABSTRACT

In the U.S., alcohol-associated liver disease (ALD) impacts millions of people and is a major healthcare burden. While the pathology of ALD is unmistakable, the molecular mechanisms underlying ethanol hepatotoxicity are not fully understood. Hepatic ethanol metabolism is intimately linked with alterations in extracellular and intracellular metabolic processes, specifically oxidation/reduction reactions. The xenobiotic detoxification of ethanol leads to significant disruptions in glycolysis, β-oxidation, and the TCA cycle, as well as oxidative stress. Perturbation of these regulatory networks impacts the redox status of critical regulatory protein thiols throughout the cell. Integrating these key concepts, our goal was to apply a cutting-edge approach toward understanding mechanisms of ethanol metabolism in disrupting hepatic thiol redox signaling. Utilizing a chronic murine model of ALD, we applied a cysteine targeted click chemistry enrichment coupled with quantitative nano HPLC-MS/MS to assess the thiol redox proteome. Our strategy reveals that ethanol metabolism largely reduces the cysteine proteome, with 593 cysteine residues significantly reduced and 8 significantly oxidized cysteines. Ingenuity Pathway Analysis demonstrates that ethanol metabolism reduces specific cysteines throughout ethanol metabolism (Adh1, Cat, Aldh2), antioxidant pathways (Prx1, Mgst1, Gsr), as well as many other biochemical pathways. Interestingly, a sequence motif analysis of reduced cysteines showed a correlation for hydrophilic, charged amino acids lysine or glutamic acid nearby. Further research is needed to determine how a reduced cysteine proteome impacts individual protein activity across these protein targets and pathways. Additionally, understanding how a complex array of cysteine-targeted post-translational modifications (e.g., S–NO, S-GSH, S–OH) are integrated to regulate redox signaling and control throughout the cell is key to the development of redox-centric therapeutic agents targeted to ameliorate the progression of ALD.

1. Introduction

In the U.S., alcohol-associated liver disease (ALD) impacts millions and is a major healthcare burden, with nearly $50 billion annually in medical expenses [1]. While the pathology of ALD is unmistakable, with marked steatosis, inflammation, and end-stage cirrhosis, the molecular mechanisms underlying ethanol hepatotoxicity are not fully understood [2,3]. Oxidative stress and mitochondrial dysfunction are reported to be significant contributors to the onset and progression of ALD [4–8]. Oxidative stress is defined as a disruption of redox signaling and control that occurs through discrete cellular redox pathways, typically involving thiol/disulfide systems [9]. Intracellularly, two thiol redox systems are employed to maintain thiol redox homeostasis, the thioredoxin (TRX) and glutathione (GSH) systems [10]. Implicating redox signaling as a key driver of ALD, several publications highlight TRX and GSH as protective agents against oxidative stress and preventing ALD [11–13]. Ethanol-derived acetaldehyde is a significant source of hepatic GSH depletion during the initiation of ALD, through the formation of acetaldehyde-cysteinyl-glycine conjugates [14,15]. While important, hepatic GSH:GSSG redox potentials (E_hGSSG) are not wholly responsible for maintaining cellular redox status. The cysteine (Cys) proteome has been identified as a large body of thiols with a great capacity for regulating redox stress throughout the cell. The human genome encodes approximately 214,000 Cys residues and 21,000–42,000 of these residues are proposed to be redox sensitive and readily oxidizable [16]. This "redox proteome" is central to macromolecular structure, regulation,

* Corresponding author. Skaggs School of Pharmacy and Pharmaceutical Sciences, University of Colorado Anschutz Medical Campus, 12850 E. Montview Blvd, Mail Stop C238, Aurora, CO, 80045, USA.
E-mail address: kristofer.fritz@cuanschutz.edu (K.S. Fritz).

https://doi.org/10.1016/j.redox.2023.102792
Received 9 May 2023; Received in revised form 9 June 2023; Accepted 18 June 2023
Available online 22 June 2023

and signaling during a hepatocytes life cycle and plays a role in the tolerance and adaptability to environmental challenges [17].

Recent research demonstrates that the redox proteome regulates cellular maintenance and growth, among other notable pathways [18–20]. These Cys residues elicit biological control via three basic mechanisms central to maintaining the proteome: 1) chemical alteration of active site Cys residues, 2) altering macromolecular interactions, and 3) regulating activity via modification of allosteric Cys [16]. Recent evidence suggests that the thiol redox proteome is a sentinel proteome that has evolved to monitor and react to the redox state of each subcellular compartment through multiple modes of feedback [21]. Interestingly, ethanol consumption impacts these same pathways that are tightly regulated through thiol redox signaling hubs [10]. Especially important to the redox biology of ethanol toxicity is the depletion of NADPH, which has been observed in models of ALD, limiting the reduction and recycling of GSH and TRX, thereby modulating the redox proteome [22]. The overall concept of thiol redox signaling is largely underexplored in ethanol toxicity and has major implications for multiple pathologic processes including inflammation, cell growth, and metabolism [23–25]. Here, we present a novel proteomics approach developed to quantify the hepatic cellular redox state to identify key redox hubs that maintain the potential for restoring redox balance. Defining these ethanol-targeted redox switches transforms our understanding of oxidative stress and redox regulated signaling during ethanol metabolism.

Interestingly, our work reinforces the notion that chronic ethanol metabolism disrupts thiol redox signaling and the downstream consequences of these perturbations reveal an as-yet unknown role for thiol redox signaling by ethanol toxicity. By applying a 6-week, Lieber-DeCarli, murine model of ALD to a novel click chemistry-based cysteine enrichment coupled with nano HPLC (nHPLC)-MS/MS, we were able to survey the hepatic cysteine proteome to quantify site-specific Cys redox status and reveal a largely reduced protein redox state. Significantly reduced cysteines were found on proteins across numerous major metabolic pathways, including GSH synthesis, ethanol metabolism, peroxiredoxins, nuclear factor erythroid 2-related factor 2 (Nrf2) and aryl hydrocarbon receptor (AhR) signaling, and lipid metabolism. Many of the known regulatory active sites on these proteins were found to be altered due to ethanol toxicity. Further research is needed to determine how a reduced cysteine proteome impacts individual protein activity and to understand how other cysteine-targeted post-translational modifications (e.g., S–NO, S-GSH, S–OH) are integrated to regulate ethanol-induced thiol redox signaling and control.

2. Materials and methods

2.1. Animals

All procedures involving animals were approved by the Institutional Animal Care and Use Committee of the University of Colorado and were performed in accordance with the published National Institutes of Health guidelines. C57BL6/J male mice were purchased from Jackson Laboratories. The 6-week Lieber-DeCarli ethanol study began with 12-week-old mice consuming liquid diet purchased from Bio-Serv that was composed of 45% of calories from fat, 16% of calories from protein, and the remainder from either carbohydrates or ethanol. Mice in the ethanol group began the study at 2% ethanol (v/v) and the concentration of ethanol was increased every week until 6% ethanol (v/v) for the final week as previously described [26,27]. Food consumption was measured daily and control mice were calorically matched with the ethanol mice through paired feeding.

2.2. Measurement of free thiols

Subcellular fractions of murine liver were obtained using a sucrose gradient [28]. Free thiols from cytoplasmic- or mitochondrial-enriched lysates were determined using Ellman's reagent (5,5′-dithiobis (2-nitrobenzoic acid) (DTNB)) as previously detailed [29]. Absorbance of the wells were read on a SpectraMax plate reader at 412 nm.

2.3. Labeling of reduced Cys proteome

The click chemistry Cys redox assay used here was adapted from Yang et al. [30] and Pertova et al. [31]. Murine liver was excised and 20 mg of tissue was placed in a tube containing 25 mM Tris, pH 7.4, 500 μM EDTA, 0.5% NP40 (v/v), protease and phosphatase inhibitors, 200U/mL catalase, and 100 μM alkynyl iodoacetamide (Kerafast, EVU111). Murine liver tissue was harvested with special attention being paid to getting the tissue into the above buffer quickly and the time was maintained for consistency between samples. The tissue was lysed on ice using a probe sonicator and incubated at room temperature to allow the alkynyl iodoacetamide to react with the free thiols of reduced cysteines. After 1 h, the samples were incubated with 8 mM DTT at 75 °C to reduce all unlabeled thiols. Samples were then alkylated with 100 mM iodoacetamide. The protein was precipitated using cold methanol:chloroform (4:1), pelleted by centrifugation, and then the protein pellet was washed with methanol:chloroform (1:1). The protein pellet was resuspended in 50 mM ammonium bicarbonate with 100 mM urea and protein concentration was determined.

Porcine modified trypsin was used to digest 1.7 mg of protein from each sample. Following digestion, the peptides were desalted using Oasis HLB solid phase extraction columns (Waters), washed with HPLC-grade water, and eluted with 80% acetonitrile (v/v) plus 10% methanol (v/v). Peptides were dried by vacuum centrifugation and then resuspended in 30% acetonitrile (v/v), pH 6.0. The copper-catalyzed azide-alkyne cycloaddition (CuAAC) reaction was performed using 10 mm sodium ascorbate, 1 mM TBTA, and 10 mM copper sulfate. A UV-cleavable biotin-azide was utilized in the reaction with the control samples receiving 1 mM ^{12}C-N_3-UV-biotin (EVU102) and the samples from ethanol mice receiving the heavy isotope 1 mM ^{13}C-N_3-UV-biotin (EVU102). A label swap using the two N_3-UV-biotin reagents was performed and showed no difference in labeling efficiency (Supplemental Fig. 1). The reaction was quenched with 5 mM sodium phosphate monobasic in 30% acetonitrile (v/v), pH 3.0. A control and isotopically heavy labeled ethanol sample were then immediately mixed one-to-one.

Excess CuAAC reagents were removed using strong cation exchange columns. The eluted peptides were allowed to bind to streptavidin beads overnight. The beads were then washed three times with 50 mM sodium acetate in 2 M sodium chloride, pH 4.5, and twice with water. The beads were resuspended in 25 mM ammonium bicarbonate, transferred to a glass vial, and exposed to UV light (365 nm) for 2 h. The supernatant containing the labeled peptides was collected, dried, and desalted. Following a final desalting using C18 spin tips, the samples were provided to the mass spectrometry core for nHPLC-MS/MS analysis.

2.4. Accurate mass and retention time (AMRT) library generation

A pooled sample of 1:1 mixed ^{12}C and ^{13}C clicked samples was loaded onto a 2 cm PepMap 100, nanoViper trapping column and chromatographically resolved on-line using a 0.075 × 250 mm, 2.0μ Acclaim PepMap RSLC reverse phase nano column (Thermo Scientific) using a 1290 Infinity II LC system equipped with a nanodapter (Agilent Technologies). Mobile phases consisted of water +0.1% formic acid (v/v) (A) and 90% acetonitrile (v/v) + 0.1% formic acid (v/v) (B). Samples were loaded onto the trapping column at 3.0 μL/min for 3 min at initial conditions before being chromatographically separated at an effective flow rate of 330 nl/min using a gradient of 3–8% B over 3 min, 8–30% B over 49 min, and 30–40% over 8 min for a total 60-min gradient at 40 °C. The gradient method was followed by a column wash at 75% B for 5 min. Data was collected on a 6550 Q-TOF equipped with a nano source (Agilent Technologies) operated using intensity dependent CID MS/MS to generate peptide ID's [32]. MS/MS data was collected in positive ion

polarity over mass ranges 260–1700 m/z at a scan rate of 8 spectra/-second for MS scans and mass ranges 50–1700 m/z at a scan rate of 3 spectra/second for MS/MS scans. All charge states were allowed except singly charged species were excluded from being selected during MS/MS acquisition and charge states 2 and 3 were given preference.

PEAKS Studio Proteomics Version 10.5 was used to extract, search, and summarize peptide identity results for the generation of an AMRT library [28]. Default settings were used to extract spectra without merging scans and detecting the correct precursor with mass only. Peptide identifications were performed using the PEAKS DB search engine combined with PEAKS de novo sequencing. Extracted spectra were searched against the SwissProt Mus musculus database using semi-specific trypsin enzyme allowing up to 2 missed tryptic cleavages with variable carbamidomethyl (Cys; +57.0215), deamidated (Asn, Gln; +0.9840), oxidation (Met; +15.9949), click ^{12}C (Cys; +252.1222), and click ^{13}C (Cys; +258.1423) modifications. The monoisotopic peptide mass tolerance allowed was ±15.0 ppm and the MS/MS tolerance was ±0.05Da. Peptides were validated by setting the false discovery rate (FDR) to 0.5% and –log10 p-value, or peptide score, accordingly.

A chemical formula was generated for each identified click peptide sequence and its corresponding modifications. If an identified peptide sequence was only found to be clicked with ^{12}C or ^{13}C, then a formula for the other click modification was also generated. Therefore, every identified click peptide had a click ^{12}C formula and a click ^{13}C formula linked with the specific mass and retention time of the original identification. Overlapping click peptide identifications, i.e., different peptides that were only different due to the ^{12}C or ^{13}C modification at the same cysteine, were filtered by retention time differences. If the retention time difference between overlapping click peptide identifications was less than the absolute value of 0.15 min then the retention time was averaged for the AMRT library. Those overlapping identifications with retention time differences greater than the absolute value of 0.15 min were manually evaluated for the presence of a heavy-labeled or light-labeled co-eluting compound with a distinct mass shift of 6.02Da. The peptide identification that did have evidence of a co-eluting compound was given preference and therefore that retention time was selected for the AMRT library.

2.5. MS-only quantitation

Data was collected in positive ion polarity over mass ranges 260–1700 m/z at a scan rate of 1.5 spectra/second on a 6550 Q-TOF equipped with a nano source (Agilent Technologies) operated in MS-only mode. One-to-one mixed ^{12}C and ^{13}C clicked samples were acquired using the same LC method and source parameters as the pooled samples for AMRT library generation.

2.6. General protein quantitation

Liver tissues from the same mice used for the thiol redox proteomics were resuspended in 3% acetonitrile (v/v) + 0.1% formic acid (v/v) in water for LC-MS and LC-MS/MS analysis. A bicinchoninic acid assay was performed to confirm peptide solution concentration and each sample was then equalized and analyzed at a final concentration of 1.2 μg/μL. Aliquots from control and ethanol samples were pooled separately and then were analyzed by LC-MS/MS for peptide identification. Remaining individual control and ethanol samples were analyzed by LC-MS-only for peptide quantitation. Here, 13.2 μg of hepatic peptides was resolved online using a 2.1 × 250 mm, 2.7 μm Advance bio peptide mapping column (Agilent) using a 1290 Infinity II LC system (Agilent). Mobile phases consisted of water +0.1% formic acid (v/v) (A) and 90% aq. Acetonitrile (v/v) + 0.1% formic acid (v/v) (B) at a flow rate of 0.25 mL/min using a gradient holding 5% B over 1 min, 5–28% B over 86 min, 28–40% B over 10 min for a total 97-min gradient at 50 °C followed by a column wash at 90% B for 5 min and re-equilibration step. Data were collected on a 6550 Q-TOF with dual AJS source (Agilent), using intensity-dependent CID MS/MS for peptide identification and library, and in MS-only mode for protein quantitation. MS/MS data were collected in positive ion mode across 270–1700 m/z at a scan rate of 8 spectra/second for MS scans and 50–1700 m/z at a scan rate of 3 spectra/second for MS/MS scans. All charge states, excluding singly charged, were allowed during MS/MS acquisition. Charge states of 2 and 3 were given preference. MS-only data were collected in positive ion mode over mass ranges 270–1700 m/z at a scan rate of 1.5 spectra/second.

PEAKS Studio Proteomics Version 10.5 was used to extract, search, and summarize peptide identity results for the generation of an AMRT library as detailed above. Extracted spectra were searched against the SwissProt Mus musculus database using semi-specific trypsin enzyme allowing up to 2 missed tryptic cleavages with variable carbamidomethyl (Cys; +57.0215), deamidated (Asn, Gln; +0.9840), and oxidation (Met; +15.9949) modifications. The monoisotopic peptide mass tolerance allowed was ±15.0 ppm and the MS/MS tolerance was ±0.05Da. Peptides were validated by setting the false discovery rate (FDR) to 1.0% and –log10 p-value, or peptide score, accordingly.

2.7. Data analysis

MS Quantitation data was extracted and aligned using Profinder V0.100.0 software (Agilent Technologies) for both the general protein quantitation and thiol redox proteomics. Retention times, neutral masses, and chemical formulas from the AMRT library were used to perform a batch targeted feature extraction [33]. Samples were extracted with an ion count threshold set to two or more ions and, for the thiol redox proteomics, 12,000 counts and a score threshold of 70. For the general protein quantitation 15,000 counts and a score threshold of 70 was used. The score is based on how the quality of the mass, isotope abundances, and isotope spacing of compounds found in each sample match to a targeted chemical formula within a specified retention time window generated form the AMRT library. Charge states 2–6 were allowed with H^+ adducts using the peptide isotope model. The thiol redox proteomics used retention time window and mass window alignment setting tolerances that were set to 0.4 min and 10 ppm, respectively. The general protein quantitation used a 0.3 min retention time window and 10 ppm mass window alignment setting tolerance.

Area counts of extracted clicked peptides were corrected by the general protein quantitation data results. Clicked peptides identified as coming from proteins that were quantified with 2 or more unique peptides in the general protein quantitation results were normalized to the relevant relative protein fold change (FC) within each sample. If the clicked peptides did not have a corresponding peptide found in the general protein quantitation, the unnormalized value was reported. Sample Control 3 was used as the reference sample for all relative protein fold changes. ^{13}C peptide area signal was corrected to 104.2% of uncorrected signal to account for the 4.2% ^{12}C impurity in the heavy labeled ^{13}C reagent as measured by direct injection LC-MS analysis (Supplemental Fig. 2). Assay validation provided in the Supplemental Figures ensured rigor and reproducibility for follow-up analysis.

Peptides were rolled up into protein data using a total area sum for all peptides matched to a specific protein. Final general protein quantitation-corrected clicked peptide data were exported to Mass Profiler Professional V.15.1 (Agilent Technologies) for statistical analysis. For the general protein quantitation, final extraction and alignment results were rolled up to protein level data were also exported to Mass Profiler Professional V.15.1 and peak areas were used for quantitation. Statistical analysis was performed at the peptide level for the thiol redox proteomics, and at the protein level for the general protein quantitation. Compounds were filtered to those found in 100% of one of two conditions. Proteins or peptides were filtered on volcano plots using a moderated *t*-test and that had a fold change >1.5 and passed a Benjamini-Hochberg multiple testing correction $p < 0.05$ were considered significant.

2.8. Enrichment analysis

Cysteine proteomic data was condensed to the protein level by combining modified peptide abundance values. Protein identifications mapped from proteins with significantly modified cysteines were used to identify strongly associated canonical pathways, and toxicity phenotypes using Ingenuity Pathway Analysis (IPA) Software (QIAGEN). Expression analysis was used to identify overlapping proteins from the Ingenuity knowledge base reference set. A right-tailed Fisher's exact test ($p < 0.05$) was used to identify significantly enriched pathways. The activation z-score, calculated by IPA, predicted activation or inhibition of canonical pathways. A z-score >0 describes an 'activated' pathway, conversely a z-score <0 describes an 'inhibited' pathway. The z-scores ≥ 2 or ≤ -2 are considered significant by IPA for predicted activation and inhibition, respectively. Cellular pathways lacking a z-score calculation signify that IPA lacked sufficient information to predict the activation state.

Subcellular pathway enrichment was conducted on the significantly changed proteins found between control and ethanol treated groups using Database for Annotation, Visualization and Integrated Discovery (DAVID) cellular component functional annotation [34]. To distinguish proteins enriched for multiple locations, Uniprot and The Human Protein Atlas were used to verify the most reported subcellular location for a given protein.

The heatmap was generated from raw abundance values of the Cys proteomic data. The top 30 most significant peptides found in all samples were included in the analysis. Graphics were generated using R studio 4.2.1 and the R-packages ggplot2 and gplots [35].

2.9. Sequence motif generation

The seven amino acids flanking the Cys residue that was significantly reduced were obtained from Uniprot. If the Cys position within the protein precluded seven flanking amino acids, that peptide was excluded from the analysis. A total of 586 peptide sequences containing cysteines that were reduced were uploaded to pLogo for sequence motif generation [36].

2.10. Immunoblotting

Murine hepatic whole tissue lysate was separated on reducing, denaturing polyacrylamide gels. Ponceau S was used to visualize the total protein loaded and normalize the signal from specific antibodies. The anti-biotin antibody was purchased from Cell Signaling Technology (7075) and was used at 1:1000 dilution. Blots were visualized using a Bio-Rad ChemiDoc MP Imaging System and analyzed using Bio-Rad ImageLab 6.0.1 software.

2.11. Statistical analysis

Statistical analyses and production of graphs were completed using GraphPad Prism 7. Analysis of control and ethanol group samples were calculated using the unpaired Student's t-test. Results were considered significant if $p < 0.05$. The unpaired *t*-test was chosen instead of the paired *t*-test because the coefficients of variation for mean food consumption were all less than 10%. For Western blot densitometry, graphs represent the average of the two groups ($n = 6$) with error bars indicating the standard deviation.

3. Results and discussion

3.1. Chronic ethanol consumption increases protein free thiols

The effect of chronic ethanol consumption on the global hepatic oxidation/reduction (redox) state of Cys was initially quantified using an Ellman's assay. Quantitation of subcellular free sulfhydryls from the ethanol-fed mice demonstrated a 12% and 27% increase in the cytoplasmic enriched and mitochondrial enriched lysates, respectively, compared to pair-fed control mice (Fig. 1A). A click chemistry reaction using alkynyl iodoacetamide and biotin-azide was also utilized to visualize proteins with reduced or oxidized cysteines via immunoblot (Fig. 1B). Our analyses showed hepatic proteins with an increased number of reduced cysteines due to chronic ethanol consumption (Fig. 1C and D). The ability to accurately identify changes in the number of reduced cysteines was verified using a chemically reduced lysate (Supplemental Fig. 3). This alternative approach validated our results and revealed a negligible change in the number of oxidized cysteines due to ethanol consumption.

3.2. Global cysteine proteome is reduced due to ethanol metabolism

Based upon our initial data indicating that ethanol metabolism induces a reduced redox state within the thiol redox proteome, we employed a proteomics approach to identify and quantify specific cysteines in the thiol redox proteome via mass spectrometry. Our click chemistry protocol was adapted to quantify protein cysteine residues that were redox modified following ethanol consumption by nHPLC-MS/MS (Fig. 2A). Employing isotopically labeled biotin-azide and combining peptides 1:1 from the pair-fed control mouse with peptides from the ethanol-fed mouse, characteristic spectra were quantified (Fig. 2B). The use of the ^{13}C-labeled biotin-azide for samples from the ethanol group resulted in an accurate and reproducible shift of the spectra by specific mass units when compared to the control peptide's spectra. To control for any changes in protein abundance, general protein quantitation was performed on the individual samples. The changes in protein abundance resulting from chronic ethanol consumption can be seen in the heatmap in Supplemental Fig. 5 with expected increases seen in proteins like Cyp2e1 (Supplemental File 1). The appropriate fold change abundance from the general protein quantitation was used to normalize the cysteine peptides from the redox proteomics dataset for each sample. A total of 938 peptides from 606 proteins were identified by mass spectrometry to have a unique labeled cysteine. Of those, 593 peptides contained cysteines that had a redox-state fold-change greater than 1.5 and were significantly reduced due to chronic ethanol consumption (red in Fig. 3A). In contrast, 8 peptides included cysteines that had a redox-state fold-change greater than 1.5 and were significantly oxidized due to ethanol consumption. Additionally, there were 235 peptides that included a cysteine redox change that met the fold change cut-off of 1.5 but did not pass the multiple comparison-corrected p-value cut-off. The effect of chronic ethanol consumption on the redox state of the hepatic cysteine proteome is shown in the heatmap, and the grouping of the ethanol mice in the principal component analysis are shown in Supplemental Fig. 6.

3.3. Ethanol consumption affects cysteine redox across subcellular compartments

The proteins identified in the cysteine redox proteomics dataset were further characterized by their subcellular localization. Ethanol metabolism disrupts the chemical biology milieu of subcellular redox potentials, such as altered NAD^+:NADH, $NADP^+$:NADPH and GSH:GSSG with implications for cell signaling in each specific cellular compartment [37–39]. A more reduced NAD^+:NADH ratio, but a more oxidized GSH:GSSG redox potential has been observed with this chronic ethanol model [38,40]. Importantly, our results define the cysteine redox proteome as a central sensor of ethanol-induced alterations in redox potentials. The cytosol and mitochondrion were the two subcellular spaces with the largest number of proteins identified (Fig. 3B). The percentages of proteins that contain a cysteine that was more reduced, oxidized, or unchanged are displayed by subcellular compartment in Fig. 3C. All the subcellular compartments had greater than 58% of the identified proteins with a cysteine that was more reduced due to chronic ethanol

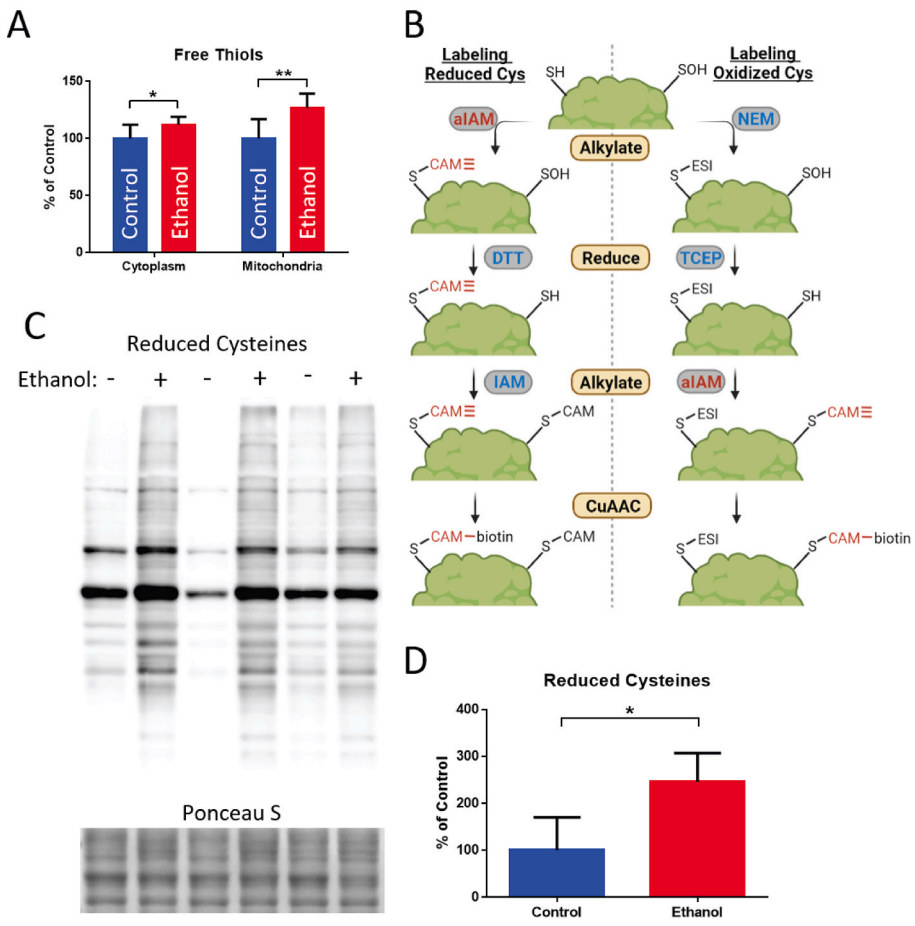

Fig. 1. Free protein thiols are increased with chronic ethanol consumption. A) Ellman's assay demonstrates increased free thiols due to chronic ethanol in both the cytoplasmic and mitochondrial enriched murine hepatic lysates. B) Schematic for labeling reduced or reversibly oxidized cysteines on proteins utilizing click chemistry to react alkynyl iodoacetamide with biotin-azide. C) A Western blot using an anti-biotin antibody demonstrates an increased number of proteins that contain a reduced cysteine. The reduced cysteines were labeled as shown on the left side of the schematic. D) Quantitation for the Western blot, after normalization to Ponceau S staining, shows a 146% increase for the reduced protein cysteines due to ethanol consumption. aIAM: alkynyl iodoacetamide; NEM: N-ethylmaleimide; CAM: carbamidomethyl; ESI: ethylsuccinimido; DTT: dithiothreitol; TCEP: tris (2-carboxyethyl)phosphine hydrochloride; IAM: iodoacetamide; *p < 0.05; **p < 0.01.

consumption. Ethanol feeding resulted in only 1% of the mitochondrion and 0.5% of the cytosolic proteins identified to be more oxidized.

3.4. Sequence motif analysis of redox altered cysteines

To determine amino acid sequence motifs corresponding to the redox change of a cysteine due to ethanol exposure, the reduced peptide dataset was uploaded to the sequence motif visualizer pLogo. If the redox altered cysteine was located near the beginning or end of the protein sequence and could not be centered in the 15 amino acid sequence, it was excluded. The peptides that contained a reduced cysteine showed a correlation for hydrophilic, charged amino acids, lysine or glutamic acid, at position +7 (Fig. 3D). This suggests an amino acid sequence motif for proteins that may be reduced due to chronic ethanol consumption of CXXXXXXK or CXXXXXXE. Of the peptides uploaded, 124 peptides containing a significantly reduced cysteine that fit one of these two motifs. While our analyses revealed a specific amino acid motif for reduced cysteines, future studies may reveal that certain cysteines are more susceptible to modification due to tertiary, quaternary, or macromolecular protein dynamics.

3.5. Pathway analysis of ethanol-induced redox proteomics

Ingenuity Pathway Analysis (IPA) of the differentially reduced or oxidized proteins demonstrated an activation of a variety of canonical pathways (Fig. 4A). Reassuringly, "Oxidative Ethanol Degradation III," "Ethanol Degradation II," and "Ethanol Degradation IV" pathways were all activated in our model (positive z-score). The three most significant pathways inhibited (negative z-score) were: "LPS/IL-1 Mediated Inhibition of RXR Function," "Mitochondrial Dysfunction," and "Sirtuin Signaling." The pathways with the highest positive z-score (activated) were "Xenobiotic Metabolism PXR Signaling" and "Xenobiotic Metabolism CAR Signaling". Interestingly, both pathways have been shown to participate in hepatic steatosis through the upregulation of lipogenesis [41–43]. Pregnane X receptor (PXR) and constitutive androstane receptor (CAR) are nuclear receptors that regulate cytochrome P450 transcription, in addition to other xenobiotic metabolism proteins [44]. Mice lacking PXR that were subjected to an 8-week ethanol diet demonstrated decreased steatosis and decreased serum ALT levels [45]. A full list of the canonical pathways, as well as the molecules identified in that pathway, are found in Supplemental File 1.

The toxicity functions identified from the IPA analyses revealed expected hepatic toxicity endpoints, but interestingly also identified several kidney injury toxicity endpoints. A previous publication from our laboratory has shown that a different post-translational modification, lysine acetylation, is also involved in ethanol-induced kidney injury through a redox effect [26]. Indeed, the toxicity functions contained several liver specific pathways and validates our methodology (Fig. 4B). Particularly of note was that 8 proteins (Cat, Gclc, Gnmt, Gstm5, Gstp1, Gstt1, Gstt2/Gsst2b, Xdh) found by our analysis are involved in "Glutathione Depletion in Liver" (Supplemental File 1). The heat map in Fig. 4C compares proteins important to the pathways identified by IPA and the specific cysteine significantly reduced or oxidized across our control and ethanol cohorts. Additional proteomic and statistical analysis for specific canonical pathways and toxicity functions can be found in Supplemental File 1.

The three proteins that had a cysteine site with the largest fold redox change were Tkfc (20.0), Aldh1l1 (14.8), and Aldob (14.8) (Supplemental File 1). Chronic alcohol consumption has been reported to change the expression of Aldh1l1 in alcoholic cirrhosis patients

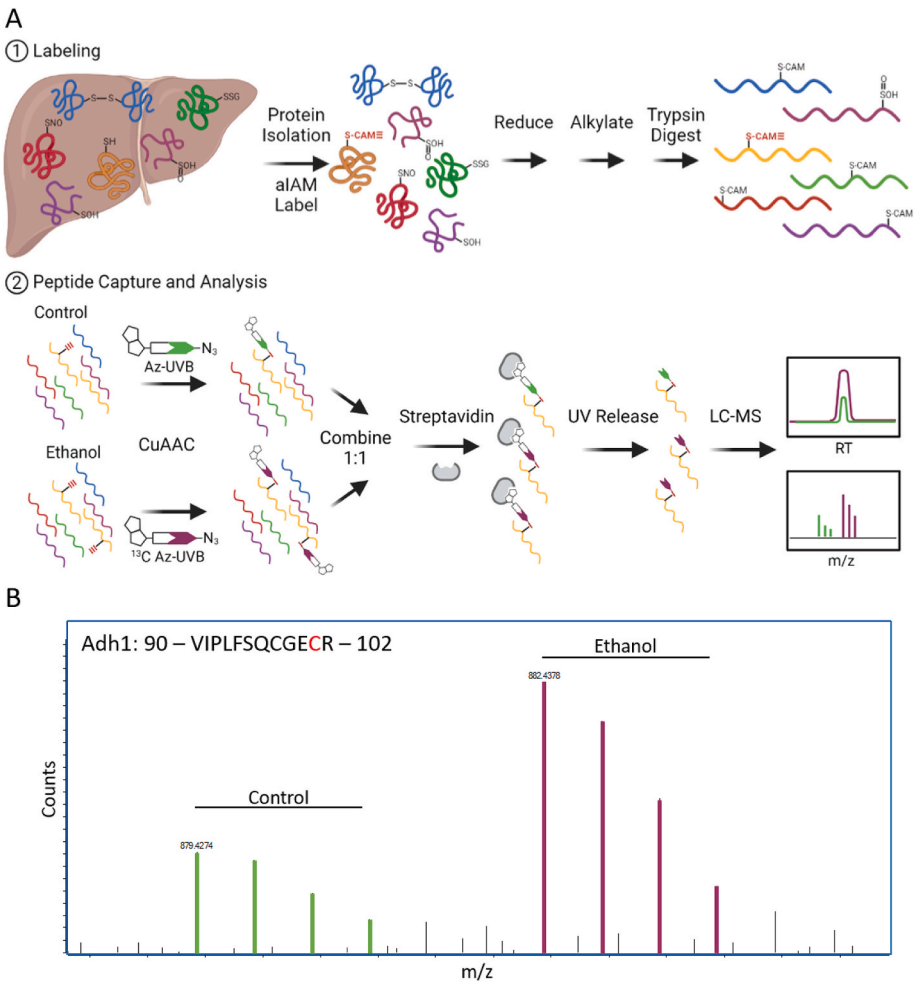

Fig. 2. Utilizing mass spectrometry to identify specific changes in the cysteine proteome. A) Schematic for the identification of reduced cysteines by mass spectrometry utilizing an alkynyl iodoacetamide (aIAM) and copper-catalyzed azide-alkyne cycloaddition (CuAAC). The red carbamidomethyl with three lines (CAM) represents the thiols labeled with the aIAM. An unlabeled and ^{13}C-labeled UV cleavable biotin-azide (Az-UVB) is used to differentiate the signal from the two samples in the same mass spectrometry injection. B) A representative mass spectrum identifying the more reduced click-chemistry labeled Cys101 (red) of Adh1 in the ethanol sample than the control sample. (For interpretation of the references to colour in this figure legend, the reader is referred to the Web version of this article.)

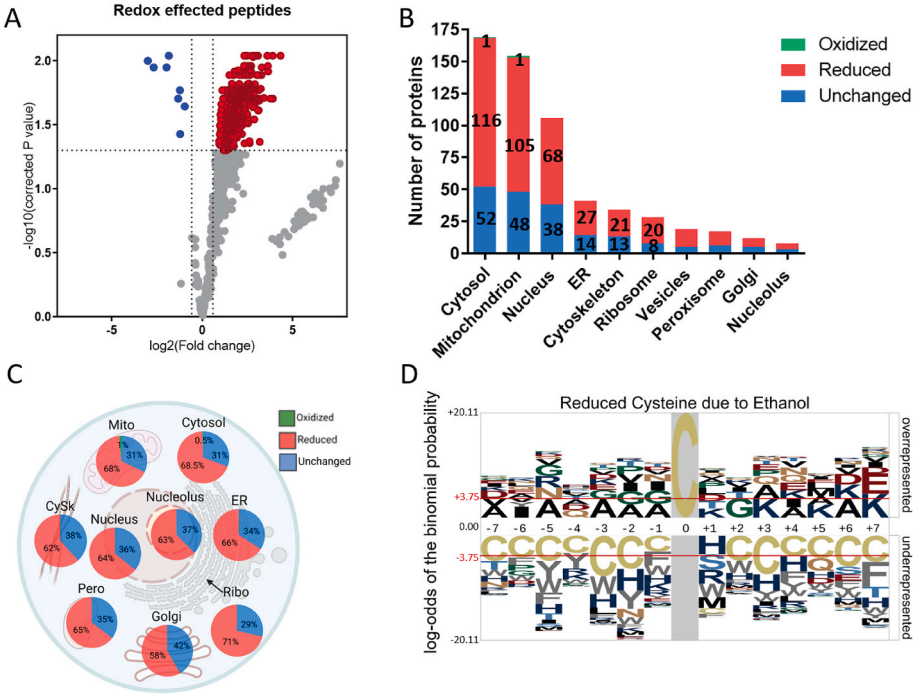

Fig. 3. Mass spectrometry identifies a significant number of reduced cysteines due to chronic ethanol consumption. A) The volcano plots depict 593 peptides that contain a significantly reduced Cys (red) and 8 peptides that contain a significantly oxidized Cys (blue) due to ethanol. B) The bar graph reports the total number of proteins in different regions of the cell that contain cysteines that were identified by mass spectrometry. The numbers report proteins that are oxidized, reduced, or unchanged due to chronic ethanol consumption. C) The percentage of proteins identified with a reduced, oxidized, or unchanged cysteine in the redox proteomics dataset varies in the different subcellular compartments. Mito: mitochondrion; CySK: cytoskeleton; Pero: peroxisome. ER: endoplasmic reticulum Ribo: ribosome. D) The pLogo sequence motifs of peptides that contain a cysteine that was reduced in the chronic ethanol group. (For interpretation of the references to colour in this figure legend, the reader is referred to the Web version of this article.)

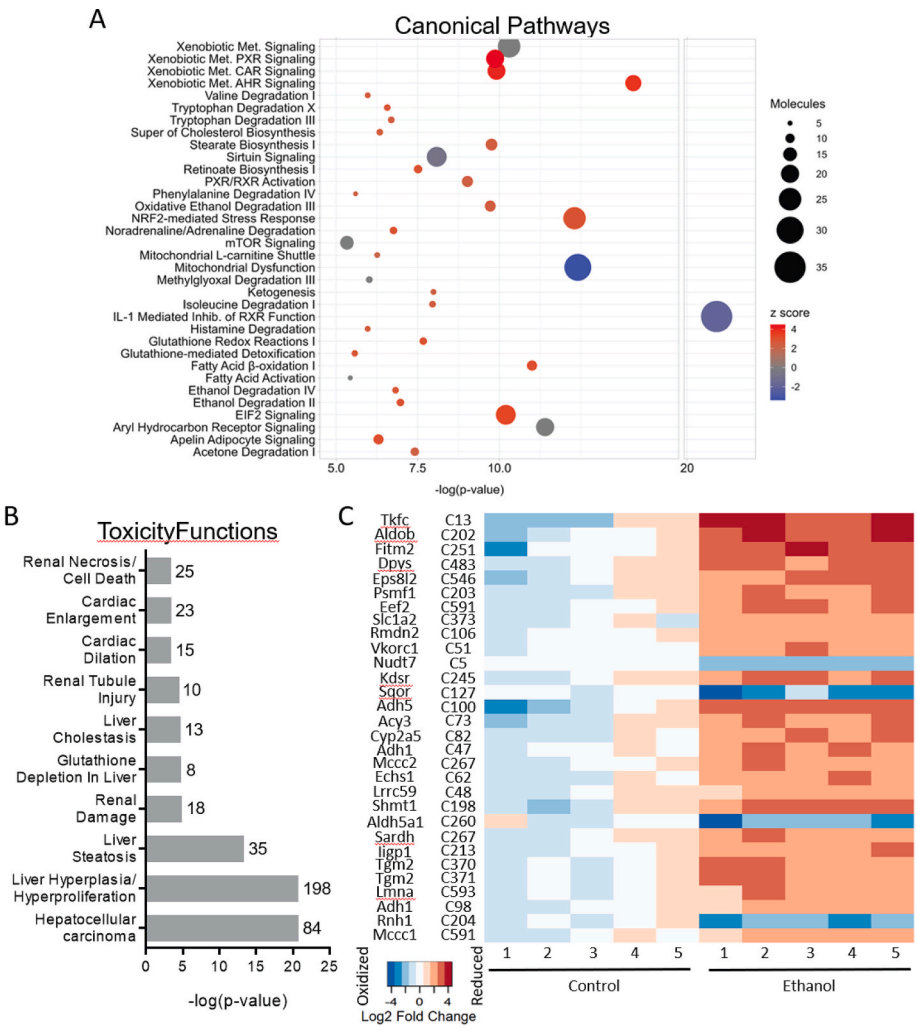

Fig. 4. Pathways affected by redox altered cysteines. A) The canonical pathways identified with -log (p-value) displaying enrichment score and z-score that demonstrates pathway activation (red), inhibition (blue) or no directionality (grey). The size represents the number of molecules found associated with the pathway. B) The toxicity endpoints with -log (p-value) showing the enrichment score and the number of molecules that are associated to the right of each pathway's bar. C) Heatmap of the top 30 peptides most significantly changed listed in decreasing statistical significance. (For interpretation of the references to colour in this figure legend, the reader is referred to the Web version of this article.)

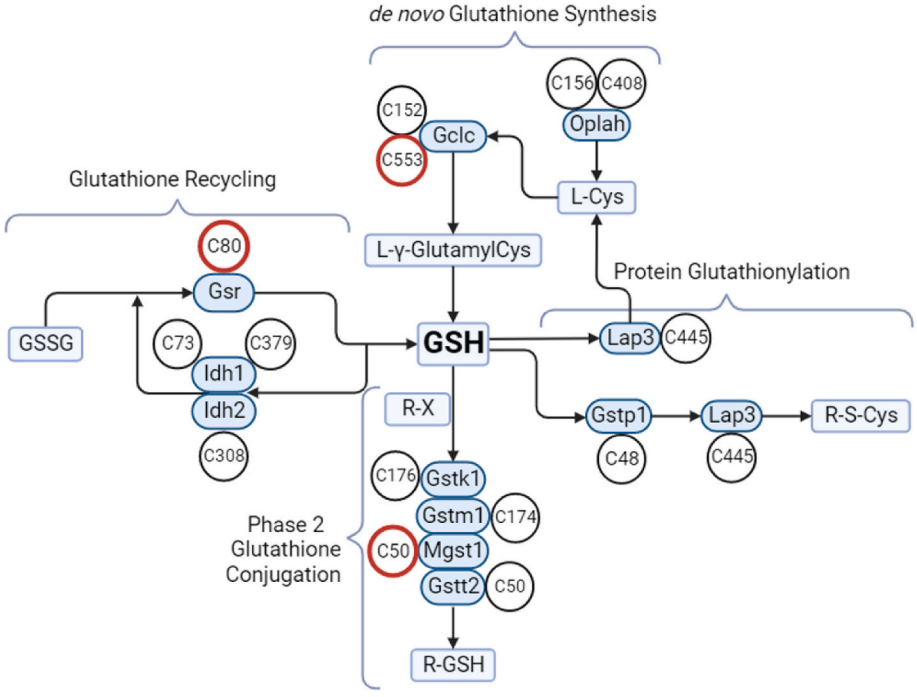

Fig. 5. Cysteine redox and glutathione metabolism. Depicted are enzymes containing significantly reduced cysteines involved with glutathione metabolism and phase two metabolism. Enzymes are labeled with their cysteines identified by redox proteomics and circled in red if the cysteine is functionally active. C/Cys: cysteine; Gclc: glutamate-cysteine ligase catalytic subunit; GSH: glutathione; GSSG: oxidized glutathione; Gsr: glutathione reductase; Gst: glutathione S-transferase; Idh: isocitrate dehydrogenase; Lap3: cytosol aminopeptidase; Mgst: microsomal glutathione S-transferase; Oplah: 5-oxoprolinase; R: organic functional group; X: halogen. (For interpretation of the references to colour in this figure legend, the reader is referred to the Web version of this article.)

receiving a liver transplant [46]. Similarly, a change in protein abundance of Aldh1l1 was observed with murine consumption of ethanol. Even when accounting for this change in Aldh1l1 abundance with the use of the general protein quantitation data, the 9 cysteines identified by redox proteomics were all significantly reduced (C86, C152, C238, C404, C451, C662, C686, C707, C774). Previously, chronic ethanol ingestion in rats was shown to decrease Aldh1l1 activity [47]. The authors of the study postulated that protein or DNA methylation might explain the change in enzyme activity. Based on our findings, another potential mechanism may be redox regulation, as C707 is one of the enzyme's active sites and C86 is adjacent to the substrate binding site.

3.6. Glutathione metabolism and cysteine redox

GSH metabolism was prominently enriched in both the canonical pathways and toxicity functions. Given the significant role GSH redox plays in ALD, these proteins were further scrutinized. Eleven different proteins and their role in GSH metabolism are illustrated in Fig. 5. Three separate pathways were also identified using IPA ("Glutathione-mediated Detoxification," "Glutathione Redox Reactions I," and "Formaldehyde Oxidation II (Glutathione-dependent)"). Two different cysteines on glutamate cysteine ligase (Gclc), the rate limiting enzyme of GSH synthesis, were found significantly reduced. Cysteine 553 of Gclc has been shown to be important for holoenzyme formation by an intermolecular disulfide bond with the modulatory subunit Gclm [48,49]. This suggests there may be a decrease in Gclc enzymatic activity elicited by a more reduced cysteine 553 due to chronic ethanol consumption. Importantly, the abundance of Gclc is not changed with ethanol consumption (Supplemental File 1). Two additional enzymes were observed to have their functionally relevant cysteines significantly reduced, glutathione reductase (Gsr) and microsomal glutathione S-transferase (Mgst1) (Fig. 5). Cysteine 80 of Gsr is part of the nucleotide binding region of the protein and is critically involved in reducing oxidized GSH disulfide to the sulfhydryl form. The activation site of Mgst1 includes cysteine 50, which was also significantly reduced in the ethanol consuming mice and is likely an inhibitory event [50].

The relationship between ethanol metabolism and decreased GSH was reported as far back as 1977 [51]. Despite the well-published effect ethanol has on GSH, a therapeutic benefit of supplementing GSH levels has yet to be realized. One clinical trial that tested the benefit in administering the antioxidant N-acetylcysteine to reduce levels of free radicals and re-establish GSH homeostasis found no difference in mortality in severe alcohol-associated hepatitis (AH) patients [52]. A recent review on GSH redox in ALD and other hepatic disease states concluded that GSH and GSH-related medications may be beneficial in combination with other treatment avenues [14]. However, the authors also noted that the exact role GSH plays in the biochemical genesis of liver pathologies remains unknown, particularly since it plays many additional roles in biology aside from a reactive oxygen species scavenger. Indeed, the reduction of these critical cysteine residues in the chronic model of ALD used here likely plays a role as a compensatory response to alcohol toxicity and reveals novel mechanisms of alcohol-induced redox signaling and control that require further investigation in this and other models [53].

3.7. Critical cysteines of ethanol metabolizing proteins are reduced

Fig. 6 depicts four key proteins involved in ethanol metabolism and the cysteine residues of those proteins that were found to be significantly reduced. Alcohol dehydrogenase 1 (Adh1) is involved in the oxidative metabolism of ethanol to acetaldehyde and has functionally relevant cysteines reduced by chronic ethanol consumption. The four functional cysteines of Adh1 bind zinc, whereby ethanol-induced Cys reduction demonstrates the absence of bound zinc and subsequent decrease in Adh1 activity in response to ethanol toxicity [54]. Specifically, cysteine 47 and cysteine 175 are defined in the UniProt database as catalytic

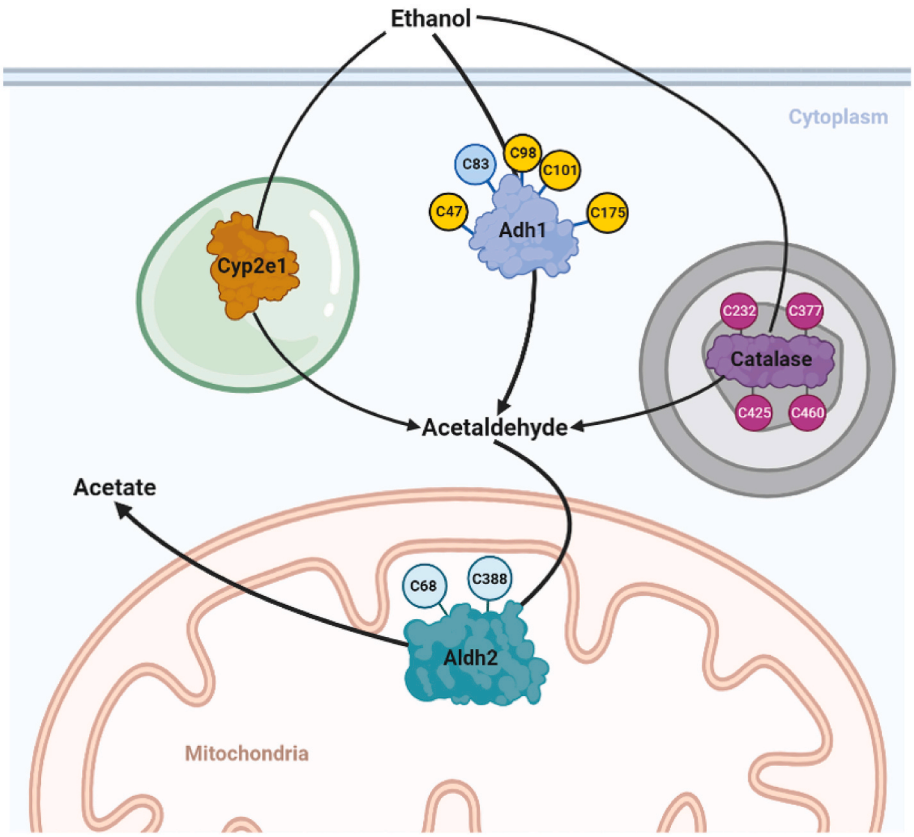

Fig. 6. Redox altered cysteines in the ethanol metabolism pathway. A) Schematic of the proteins involved in ethanol metabolism and the cysteines (e.g., C83) identified to be significantly reduced in the redox proteomics dataset. The cysteines highlighted in yellow have a known functional role. Cyp2e1: cytochrome P450 2E1; Adh1: alcohol dehydrogenase 1; Aldh2: aldehyde dehydrogenase 2. (For interpretation of the references to colour in this figure legend, the reader is referred to the Web version of this article.)

amino acids of Adh1 and may be key targets in this response. Utilizing iodoacetamide in our Cys capture method prevents displacement of Cys-bound zinc, thus labeling unbound Cys and indicating enzyme inhibition [55]. It remains difficult to determine if Cys oxidation/reduction is inhibitory or activating on a global scale and requires a thorough case-by-case analysis to fully interpret how specific redox changes alter protein function. The protein abundance of most ethanol metabolizing enzymes was unchanged between control and ethanol-fed mice, except for the expected increase in Cyp2e1 in response to chronic ethanol consumption (Supplemental File 1). Adjusting for the increased abundance of Cyp2e1 results in two cysteines of the protein, C261 and C437, to fall outside of the p-value cutoff. It is worth noting that cysteine 437 of Cyp2e1 participates in iron binding and the observed reduction may support the previously demonstrated increased activity in this chronic model [56]. The rate limiting enzyme in ethanol metabolism, aldehyde dehydrogenase 2 (ALDH2), also contained two thiols that were more reduced in the ethanol group, cysteine 68 and cysteine 388. This contrasts with previous work that used two-dimensional gel-based proteomics to report the oxidation of ALDH2 protein as a whole [57]. Indeed, functional redox assays coupled to MS analysis will be necessary for a case-by-case determination of total protein oxidation/reduction and site-specific changes in the context of protein activity.

Overall, the observed increase in reduced cysteines due to chronic ethanol consumption is supported by the chemistry of ethanol as a reducing agent [58]. The conversion of ethanol to acetaldehyde results in ethanol losing two electrons and the reduction of NAD^+ to NADH, shifting the NAD^+:NADH redox ratio within the hepatocyte [38]. Altered NAD^+:NADH redox ratios have been identified as an important component to redox equilibrium [59]. This balance is also critical for coordinating nutrient shuttling, and as a key cofactor for glycolysis, citric acid cycle, and lipogenesis. Additionally, reduction of NAD^+ to NADH also occurs when acetaldehyde is converted to acetate. Our previous work attempted to increase NAD^+ abundance through nicotinamide mononucleotide (NMN) supplementation, a NAD^+ precursor, which alleviated ethanol-induced liver damage as observed by ALT and AST [60]. It remains to be determined if NMN supplementation affects the redox state of the cysteines of ethanol metabolizing proteins.

4. Conclusions

Since the total protein thiol pool approaches 40 mM and the abundant thiol GSH is at ~5–10 mM in liver, hepatic thiols may represent a more abundant redox system capable of regulating nearly all processes throughout the cell [61]. The chemical reactivity of protein cysteine residues is highly modulated through exogenous and endogenous factors, including pH, electrolytes, and temperature [62]. Cysteines are also regarded as "order-promoting" amino acid residues due to their finely tuned mechanism of inter- and intra-molecular disulfide bonds, stabilizing proteins under oxidizing conditions [63]. Altogether, these unique features of cysteine residues enable them to sense cellular metabolism and oxidative stress to alter protein structure, function, and signaling.

To date, little is known regarding how proteomic thiol redox potentials communicate in response to ethanol toxicity. Traditional interpretations of oxidative stress and GSH redox potentials must be adapted to novel high-resolution approaches that can provide nuanced analyses of disrupted redox signaling and control at the amino acid level. Indeed, applying an updated analyses of ethanol-induced alterations in the thiol redox proteome reveals biochemical mechanisms through which protein pathways sense hepatic oxidative stress. Our redox proteomics analysis using a murine model of ALD integrates an advanced nHPLC-MS/MS redox approach to validate a global free thiol approach by Ellman's assay, which both demonstrate that the free thiols of hepatic proteins are in a more reduced state due to chronic ethanol consumption. Our previously published work revealed a redox potential for GSH that was more oxidized due to a decrease in GSH levels [40]. Interpreting the pathophysiological consequences of altered hepatic GSH levels remains difficult and presents a broad assessment of "oxidative stress" that is constrained. However, assessing GSH redox potentials is only one piece of the complex thiol redox proteome puzzle. Indeed, several cysteine modifications (e.g., S–NO, S-GSH, S–OH, cysteine carbonylation) are reportedly increased due to chronic ethanol consumption using older methodologies [64–67]. Our click chemistry-based approach provides a specific and sensitive pipeline that can be adapted to further investigate these cysteine modifications to advance the field of ethanol hepatoxicity. To gain better insight regarding the thiol redox proteome, our approach identified and quantified ethanol-induced changes in the thiol redox proteome on hepatic proteins, revealing a reduced redox proteome and specific alcohol-related redox sensing cysteine residues. Further understanding how ethanol metabolism disrupts thiol signaling and protein activity will provide key insight into the pathogenesis of ALD while uncovering novel targets for therapeutic intervention by specifically targeting certain redox signaling hubs.

Declaration of competing interest

The authors declare no conflicts of interest.

Data availability

Data will be made available on request.

Acknowledgements

This work was funded in part through NIH grants by JRR (NIEHS ES027593) and KSF (NIAAA AA026928, AA029218, AA030024), by the Skaggs Scholars program at the University of Colorado, Skaggs School of Pharmacy and Pharmaceutical Sciences (KSF), by the NIH/NCATS Colorado CTSA Grant Number TL1 TR002533 (CDM), and by the NIH P30CA046934 Bioinformatics and Biostatistics Shared Resource Core. We thank Dr. Nichole Reisdorph and the Skaggs School of Pharmacy Mass Spectrometry Core for collaboration.

Appendix A. Supplementary data

Supplementary data to this article can be found online at https://doi.org/10.1016/j.redox.2023.102792.

References

[1] World Health Organization, Global Status Report on Alcohol and Health 2014, World Health Organization, Geneva, 2014, p. 376, xiv.
[2] F.R. Sun, B.Y. Wang, Alcohol and metabolic-associated fatty liver disease, J Clin Transl Hepatol 9 (5) (2021) 719–730.
[3] R. Bataller, G.E. Arteel, C. Moreno, V. Shah, Alcohol-related liver disease: time for action, J. Hepatol. 70 (2) (2019) 221–222.
[4] S.K. Das, D.M. Vasudevan, Alcohol-induced oxidative stress, Life Sci. 81 (3) (2007) 177–187.
[5] N.A. Osna, R.L. White, S. Todero, B.L. McVicker, G.M. Thiele, D.L. Clemens, D. J. Tuma, T.M. Donohue Jr., Ethanol-induced oxidative stress suppresses generation of peptides for antigen presentation by hepatoma cells, Hepatology (Baltimore, Md 45 (1) (2007) 53–61.
[6] L. Bonet-Ponce, S. Saez-Atienzar, C. da Casa, M. Flores-Bellver, J.M. Barcia, J. Sancho-Pelluz, F.J. Romero, J. Jordan, M.F. Galindo, On the mechanism underlying ethanol-induced mitochondrial dynamic disruption and autophagy response, Biochim. Biophys. Acta 1852 (7) (2015) 1400–1409.
[7] V.V. Teplova, A.G. Kruglov, L.I. Kovalyov, A.B. Nikiforova, N.I. Fedotcheva, J. J. Lemasters, Glutamate contributes to alcohol hepatotoxicity by enhancing oxidative stress in mitochondria, J. Bioenerg. Biomembr. 49 (3) (2017) 253–264.
[8] D. Han, H.S. Johnson, M.P. Rao, G. Martin, H. Sancheti, K.H. Silkwood, C. W. Decker, K.T. Nguyen, J.G. Casian, E. Cadenas, N. Kaplowitz, Mitochondrial remodeling in the liver following chronic alcohol feeding to rats, Free Radic. Biol. Med. 102 (2017) 100–110.
[9] D.P. Jones, Redefining oxidative stress, Antioxidants Redox Signal. 8 (9–10) (2006) 1865–1879.
[10] T. Nietzel, J. Mostertz, F. Hochgrafe, M. Schwarzlander, Redox regulation of mitochondrial proteins and proteomes by cysteine thiol switches, Mitochondrion 33 (2017) 72–83.

[11] J.I. Cohen, S. Roychowdhury, P.M. DiBello, D.W. Jacobsen, L.E. Nagy, Exogenous thioredoxin prevents ethanol-induced oxidative damage and apoptosis in mouse liver, Hepatology 49 (5) (2009) 1709–1717.

[12] J.C. Fernandez-Checa, A. Colell, C. Garcia-Ruiz, S-Adenosyl-L-methionine and mitochondrial reduced glutathione depletion in alcoholic liver disease, Alcohol (N. Y.) 27 (3) (2002) 179–183.

[13] T. Hirano, N. Kaplowitz, H. Tsukamoto, S. Kamimura, J.C. Fernandez-Checa, Hepatic mitochondrial glutathione depletion and progression of experimental alcoholic liver disease in rats, Hepatology 16 (6) (1992) 1423–1427.

[14] M. Vairetti, L.G. Di Pasqua, M. Cagna, P. Richelmi, A. Ferrigno, C. Berardo, Changes in glutathione content in liver diseases: an update, Antioxidants 10 (3) (2021).

[15] H. Anni, P. Pristatsky, Y. Israel, Binding of acetaldehyde to a glutathione metabolite: mass spectrometric characterization of an acetaldehyde-cysteinylglycine conjugate, Alcohol Clin. Exp. Res. 27 (10) (2003) 1613–1621.

[16] D.P. Jones, Radical-free biology of oxidative stress, Am. J. Physiol. Cell Physiol. 295 (4) (2008) C849–C868.

[17] Y.M. Go, D.P. Jones, The redox proteome, J. Biol. Chem. 288 (37) (2013) 26512–26520.

[18] U. Topf, I. Suppanz, L. Samluk, L. Wrobel, A. Boser, P. Sakowska, B. Knapp, M. K. Pietrzyk, A. Chacinska, B. Warscheid, Quantitative proteomics identifies redox switches for global translation modulation by mitochondrially produced reactive oxygen species, Nat. Commun. 9 (1) (2018) 324.

[19] H. Xiao, M.P. Jedrychowski, D.K. Schweppe, E.L. Huttlin, Q. Yu, D.E. Heppner, J. Li, J. Long, E.L. Mills, J. Szpyt, Z. He, G. Du, R. Garrity, A. Reddy, L.P. Vaites, J. A. Paulo, T. Zhang, N.S. Gray, S.P. Gygi, E.T. Chouchani, A quantitative tissue-specific landscape of protein redox regulation during aging, Cell 180 (5) (2020) 968–983 e24.

[20] C.C. Winterbourn, Hydrogen peroxide reactivity and specificity in thiol-based cell signalling, Biochem. Soc. Trans. 48 (3) (2020) 745–754.

[21] N.S. Gould, P. Evans, P. Martinez-Acedo, S.M. Marino, V.N. Gladyshev, K. S. Carroll, H. Ischiropoulos, Site-specific proteomic mapping identifies selectively modified regulatory cysteine residues in functionally distinct protein networks, Chem. Biol. 22 (7) (2015) 965–975.

[22] Y. Liang, F.L. Harris, D.P. Jones, L.A. Brown, Alcohol induces mitochondrial redox imbalance in alveolar macrophages, Free Radic. Biol. Med. 65 (2013) 1427–1434.

[23] N. Ghasemzadeh, R.S. Patel, D.J. Eapen, E. Veledar, H. Al Kassem, P. Manocha, M. Khayata, A.M. Zafari, L. Sperling, D.P. Jones, A.A. Quyyumi, Oxidative stress is associated with increased pulmonary artery systolic pressure in humans, Hypertension 63 (6) (2014) 1270–1275.

[24] S.C. Pugliese, J.M. Poth, M.A. Fini, A. Olschewski, K.C. El Kasmi, K.R. Stenmark, The role of inflammation in hypoxic pulmonary hypertension: from cellular mechanisms to clinical phenotypes, Am. J. Physiol. Lung Cell Mol. Physiol. 308 (3) (2015) L229–L252.

[25] M. Lakemeyer, M. Bogyo, Uncovering an overlooked consequence of phosphorylation: change in cysteine reactivity, Nat. Methods 19 (3) (2022) 281–283.

[26] P.S. Harris, S.R. Roy, C. Coughlan, D.J. Orlicky, Y. Liang, C.T. Shearn, J.R. Roede, K.S. Fritz, Chronic ethanol consumption induces mitochondrial protein acetylation and oxidative stress in the kidney, Redox Biol. 6 (2015) 33–40.

[27] K.S. Fritz, J.J. Galligan, M.D. Hirschey, E. Verdin, D.R. Petersen, Mitochondrial acetylome analysis in a mouse model of alcohol-induced liver injury utilizing SIRT3 knockout mice, J. Proteome Res. 11 (3) (2012) 1633–1643.

[28] H.R. Ali, M.A. Assiri, P.S. Harris, C.R. Michel, Y. Yun, J.O. Marentette, F.K. Huynh, D.J. Orlicky, C.T. Shearn, L.M. Saba, R. Reisdorph, N. Reisdorph, M.D. Hirschey, K. S. Fritz, Quantifying competition among mitochondrial protein acylation events induced by ethanol metabolism, J. Proteome Res. 18 (4) (2019) 1513–1531.

[29] J.R. Roede, D.P. Jones, Thiol-reactivity of the fungicide maneb, Redox Biol. 2 (2014) 651–655.

[30] J. Yang, V. Gupta, K.A. Tallman, N.A. Porter, K.S. Carroll, D.C. Liebler, Global, in situ, site-specific analysis of protein S-sulfenylation, Nat. Protoc. 10 (7) (2015) 1022–1037.

[31] B. Petrova, K. Liu, C. Tian, M. Kitaoka, E. Freinkman, J. Yang, T.L. Orr-Weaver, Dynamic redox balance directs the oocyte-to-embryo transition via developmentally controlled reactive cysteine changes, Proc. Natl. Acad. Sci. U. S. A. 115 (34) (2018) E7978–E7986.

[32] H.R. Ali, C.R. Michel, Y.H. Lin, T.A. McKinsey, M.Y. Jeong, A.V. Ambardekar, J. C. Cleveland, R. Reisdorph, N. Reisdorph, K.C. Woulfe, K.S. Fritz, Defining decreased protein succinylation of failing human cardiac myofibrils in ischemic cardiomyopathy, J. Mol. Cell. Cardiol. 138 (2020) 304–317.

[33] P.S. Harris, C.R. Michel, Y. Yun, C.D. McGinnis, M.A. Assiri, A.R. Ahmadi, Z. Sun, J. R. Roede, M.A. Burchill, D.J. Orlicky, R.L. McCullough, K.S. Fritz, Proteomic analysis of alcohol-associated hepatitis reveals glycoprotein NMB (GPNMB) as a novel hepatic and serum biomarker, Alcohol (N. Y.) 99 (2021) 35–48.

[34] W. Huang da, B.T. Sherman, R.A. Lempicki, Systematic and integrative analysis of large gene lists using DAVID bioinformatics resources, Nat. Protoc. 4 (1) (2009) 44–57.

[35] H. Wickham, G. Grolemund, R for Data Science: Import, Tidy, Transform, Visualize, and Model Data, O'Reilly Media, Inc., 2016.

[36] J.P. O'Shea, M.F. Chou, S.A. Quader, J.K. Ryan, G.M. Church, D. Schwartz, pLogo: a probabilistic approach to visualizing sequence motifs, Nat. Methods 10 (12) (2013) 1211–1212.

[37] G. Vendemiale, I. Grattagliano, A. Signorile, E. Altomare, Ethanol-induced changes of intracellular thiol compartmentation and protein redox status in the rat liver: effect of tauroursodeoxycholate, J. Hepatol. 28 (1) (1998) 46–53.

[38] K.S. Fritz, J.J. Galligan, R.L. Smathers, J.R. Roede, C.T. Shearn, P. Reigan, D. R. Petersen, 4-Hydroxynonenal inhibits SIRT3 via thiol-specific modification, Chem. Res. Toxicol. 24 (5) (2011) 651–662.

[39] R.P. Goodman, S.E. Calvo, V.K. Mootha, Spatiotemporal compartmentalization of hepatic NADH and NADPH metabolism, J. Biol. Chem. 293 (20) (2018) 7508–7516.

[40] M.A. Assiri, S.R. Roy, P.S. Harris, H. Ali, Y. Liang, C.T. Shearn, D.J. Orlicky, J. R. Roede, M.D. Hirschey, D.S. Backos, K.S. Fritz, Chronic ethanol metabolism inhibits hepatic mitochondrial superoxide dismutase via lysine acetylation, Alcohol Clin. Exp. Res. 41 (10) (2017) 1705–1714.

[41] J. Zhou, Y. Zhai, Y. Mu, H. Gong, H. Uppal, D. Toma, S. Ren, R.M. Evans, W. Xie, A novel pregnane X receptor-mediated and sterol regulatory element-binding protein-independent lipogenic pathway, J. Biol. Chem. 281 (21) (2006) 15013–15020.

[42] X. Chen, Z. Meng, X. Wang, S. Zeng, W. Huang, The nuclear receptor CAR modulates alcohol-induced liver injury, Laboratory investigation; a journal of technical methods and pathology 91 (8) (2011) 1136–1145.

[43] A. Moreau, M.J. Vilarem, P. Maurel, J.M. Pascussi, Xenoreceptors CAR and PXR activation and consequences on lipid metabolism, glucose homeostasis, and inflammatory response, Mol. Pharm. 5 (1) (2008) 35–41.

[44] L.A. Stanley, B.C. Horsburgh, J. Ross, N. Scheer, C.R. Wolf, PXR and CAR: nuclear receptors which play a pivotal role in drug disposition and chemical toxicity, Drug Metab. Rev. 38 (3) (2006) 515–597.

[45] S. Choi, P. Neequaye, S.W. French, F.J. Gonzalez, M.A. Gyamfi, Pregnane X receptor promotes ethanol-induced hepatosteatosis in mice, J. Biol. Chem. 293 (1) (2018) 1–17.

[46] K. Muffak-Granero, C. Olmedo, F. Garcia-Alcalde, A. Comino, T. Villegas, J. M. Villar, D. Garrote, A. Blanco, P. Bueno, J.A. Ferron, Gene network profiling before and after transplantation in alcoholic cirrhosis liver transplant recipients, Transplant. Proc. 44 (6) (2012) 1493–1495.

[47] H. Min, E.S. Im, J.S. Seo, J.A. Mun, B.J. Burri, Effects of chronic ethanol ingestion and folate deficiency on the activity of 10-formyltetrahydrofolate dehydrogenase in rat liver, Alcohol Clin. Exp. Res. 29 (12) (2005) 2188–2193.

[48] Z. Tu, M.W. Anders, Identification of an important cysteine residue in human glutamate-cysteine ligase catalytic subunit by site-directed mutagenesis, Biochem. J. 336 (Pt 3) (1998) 675–680.

[49] D.S. Backos, K.S. Fritz, J.R. Roede, D.R. Petersen, C.C. Franklin, Posttranslational modification and regulation of glutamate-cysteine ligase by the alpha,beta-unsaturated aldehyde 4-hydroxy-2-nonenal, Free Radic. Biol. Med. 50 (1) (2011) 14–26.

[50] R. Morgenstern, J.W. DePierre, L. Ernster, Activation of microsomal glutathione S-transferase activity by sulfhydryl reagents, Biochem. Biophys. Res. Commun. 87 (3) (1979) 657–663.

[51] C.M. Macdonald, J. Dow, M.R. Moore, A possible protective role for sulphydryl compounds in acute alcoholic liver injury, Biochem. Pharmacol. 26 (16) (1977) 1529–1531.

[52] E. Nguyen-Khac, T. Thevenot, M.A. Piquet, S. Benferhat, O. Goria, D. Chatelain, B. Tramier, F. Dewaele, S. Ghrib, M. Rudler, N. Carbonell, H. Tossou, A. Bental, B. Bernard-Chabert, J.L. Dupas, A.-N.S. Group, Glucocorticoids plus N-acetylcysteine in severe alcoholic hepatitis, N. Engl. J. Med. 365 (19) (2011) 1781–1789.

[53] B. Gao, M.J. Xu, A. Bertola, H. Wang, Z. Zhou, S. Liangpunsakul, Animal models of alcoholic liver disease: pathogenesis and clinical relevance, Gene Expr. 17 (3) (2017) 173–186.

[54] Q. Hao, W. Maret, Aldehydes release zinc from proteins. A pathway from oxidative stress/lipid peroxidation to cellular functions of zinc, FEBS J. 273 (18) (2006) 4300–4310.

[55] M.D. Peris-Diaz, R. Guran, O. Zitka, V. Adam, A. Krezel, Metal- and affinity-specific dual labeling of cysteine-rich proteins for identification of metal-binding sites, Anal. Chem. 92 (19) (2020) 12950–12958.

[56] D.J. Orlicky, J.R. Roede, E. Bales, C. Greenwood, A. Greenberg, D. Petersen, J. L. McManaman, Chronic ethanol consumption in mice alters hepatocyte lipid droplet properties, Alcohol Clin. Exp. Res. 35 (6) (2011) 1020–1033.

[57] A. Venkatraman, A. Landar, A.J. Davis, E. Ulasova, G. Page, M.P. Murphy, V. Darley-Usmar, S.M. Bailey, Oxidative modification of hepatic mitochondria protein thiols: effect of chronic alcohol consumption, Am. J. Physiol. Gastrointest. Liver Physiol. 286 (4) (2004) G521–G527.

[58] P.R. Ryle, J. Chakraborty, A.D. Thomson, The roles of the hepatocellular redox state and the hepatic acetaldehyde concentration in determining the ethanol elimination rate in fasted rats, Biochem. Pharmacol. 34 (19) (1985) 3577–3583.

[59] W. Xiao, R.S. Wang, D.E. Handy, J. Loscalzo, NAD(H) and NADP(H) redox couples and cellular energy metabolism, Antioxidants Redox Signal. 28 (3) (2018) 251–272.

[60] M.A. Assiri, H.R. Ali, J.O. Marentette, Y. Yun, J. Liu, M.D. Hirschey, L.M. Saba, P. S. Harris, K.S. Fritz, Investigating RNA expression profiles altered by nicotinamide mononucleotide therapy in a chronic model of alcoholic liver disease, Hum. Genom. 13 (1) (2019) 65.

[61] Y.M. Go, D.P. Jones, Thiol/disulfide redox states in signaling and sensing, Crit. Rev. Biochem. Mol. Biol. 48 (2) (2013) 173–181.

[62] X. Liu, D.C. Dawson, Cystic fibrosis transmembrane conductance regulator: temperature-dependent cysteine reactivity suggests different stable conformers of the conduction pathway, Biochemistry 50 (47) (2011) 10311–10317.

[63] A.A. Bhopatkar, V.N. Uversky, V. Rangachari, Disorder and cysteines in proteins: a design for orchestration of conformational see-saw and modulatory functions, Prog Mol Biol Transl Sci 174 (2020) 331–373.

[64] K.H. Moon, B.L. Hood, B.J. Kim, J.P. Hardwick, T.P. Conrads, T.D. Veenstra, B. J. Song, Inactivation of oxidized and S-nitrosylated mitochondrial proteins in alcoholic fatty liver of rats, Hepatology 44 (5) (2006) 1218–1230.

[65] D. Gergel, A.I. Cederbaum, Inhibition of the catalytic activity of alcohol dehydrogenase by nitric oxide is associated with S nitrosylation and the release of zinc, Biochemistry 35 (50) (1996) 16186–16194.

[66] M.E. Price, J.A. Pavlik, M. Liu, S.J. Ding, T.A. Wyatt, J.H. Sisson, Alcohol drives S-nitrosylation and redox activation of protein phosphatase 1, causing bovine airway cilia dysfunction, Am. J. Physiol. Lung Cell Mol. Physiol. 312 (3) (2017) L432–L439.

[67] J.J. Galligan, R.L. Smathers, K.S. Fritz, L.E. Epperson, L.E. Hunter, D.R. Petersen, Protein carbonylation in a murine model for early alcoholic liver disease, Chem. Res. Toxicol. 25 (5) (2012) 1012–1021.